Atomically dispersed Fe–N–C catalyst displaying ultra-high stability and recyclability for efficient electroreduction of CO_2 to CO

Bao-Xia Dong[*], Meng-Ting Peng, Qiu-Hui Zheng, Si-Min Cao, Yun-Lei Teng[*], Di-Chang Zhong, Zong-Wei Li

School of Chemistry and Chemical Engineering, Yangzhou University, Yangzhou 225002, Jiangsu, China

Contents:

Figure S1. X-ray powder diffraction patterns of the as-synthesized precursors.

Figure S2. (a) N_2 adsorption and desorption curves of the precursors at 77K; (b) The pore size distribution in each one.

Table S1. Characterization results of N_2 adsorption and desorption of the precursors

Sample	S_{BET} (m²/g)	$S_{Langmuir}$ (m²/g)	V_{proe} (m³/g)	Micropore volume (cm³/g)	BJH desorption cumulative volume of pores in the range of 0.85–120 nm (cm³/g)
PCN-224(Zn_1Fe_0)	1548	2310	0.850	0.605	0.161

PCN-224($Zn_{0.8}Fe_{0.2}$)	2156	3205	1.156	0.857	0.198
PCN-224($Zn_{0.5}Fe_{0.5}$)	2103	3172	1.130	0.803	0.208
PCN-224(Zn_0Fe_1)	992	1445	0.518	0.399	0.064
PCN-222($Zn_{0.5}Fe_{0.5}$)	2014	3274	1.136	0.082	1.054

Table S2. The ICP and elemental analysis results of Zn_xFe_y–N–C catalysts

Sample	Fe wt%	Zn wt%	C wt%	N wt%
Zn_1Fe_0–N–C-224	0	0	55.45	2.02
$Zn_{0.8}Fe_{0.2}$–N–C-224	0.81	0	78.12	1.11
$Zn_{0.5}Fe_{0.5}$–N–C-224	1.06	0	76.93	0.92
Zn_0Fe_1–N–C-224	3.01	0	63.30	1.49
$Zn_{0.5}Fe_{0.5}$–N–C-222	1.04	0	81.94	0.93
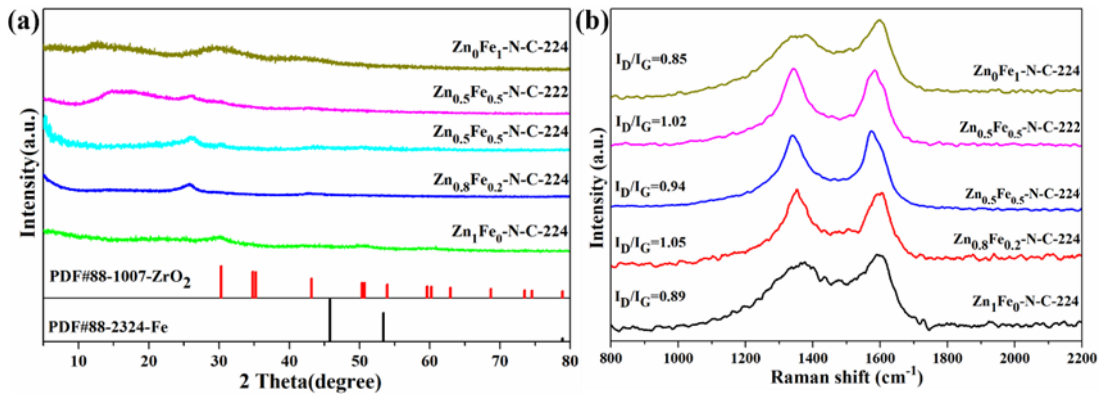
Figure S3. X-ray powder diffraction patterns (a) and Raman spectra (b) of Zn_xFe_y–N–C catalysts derived from different precursors.

The intensity ratios (I_D/I_G) of the D-band (~1345 cm^{-1}) and the G-band (~1590 cm^{-1}) in $Zn_{0.8}Fe_{0.2}$–N–C-224, $Zn_{0.5}Fe_{0.5}$–N–C-224, and $Zn_{0.5}Fe_{0.5}$–N–C-222 were 1.05, 0.94, and 1.02, respectively, much higher than those of Zn_0Fe_1–N–C-224 (0.85) and Zn_1Fe_0–N–C-224 (0.89), projecting their effective electron transportability (Fig. S3b).
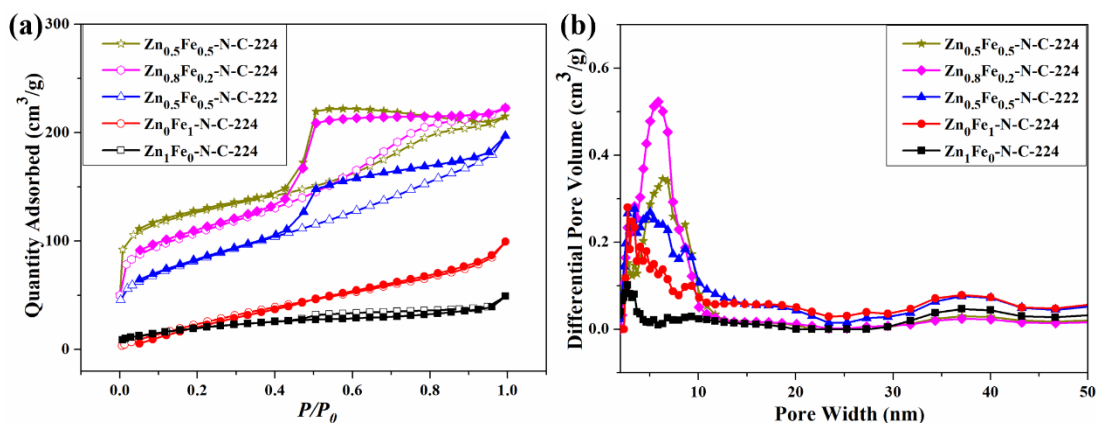
Figure S4. (a) N_2 sorption isotherms at 77 K for Zn_xFe_y–N–C catalysts; (b) The DFT pore size distribution of each sample.

Table S3. The specific surface area and pore volume for the Zn_xFe_y–N–C materials

Sample	S_{BET} (m²/g)	$S_{Langmuir}$ (m²/g)	V_{proe} (cm³/g)	Micropore volume (cm³/g)	BJH desorption cumulative volume of pores in the range of 0.85–120 nm (cm³/g)
Zn_1Fe_0–N–C-224	75	122	0.077	0.010	0.066
$Zn_{0.8}Fe_{0.2}$–N–C-224	366	560	0.345	0.048	0.293
$Zn_{0.5}Fe_{0.5}$–N–C-224	411	617	0.332	0.103	0.227
$Zn_{0.5}Fe_{0.5}$–N–C-222	291	450	0.305	0.008	0.280
Zn_0Fe_1–N–C-224	125	287	0.154	0.052	0.137
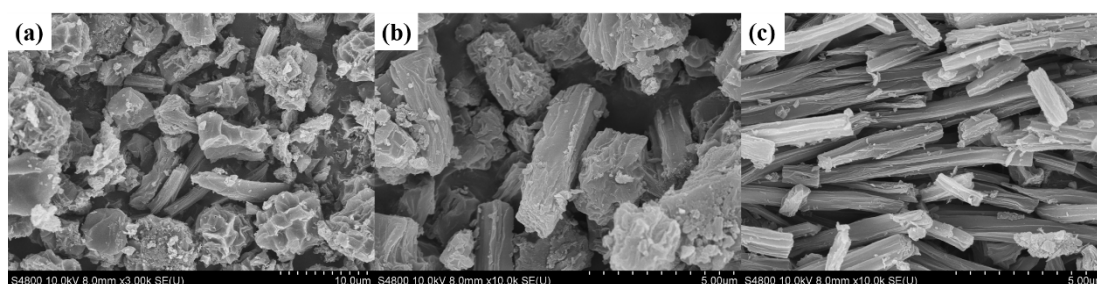
Figure S5. The SEM images of Zn_xFe_y–N–C: (a) $Zn_{0.8}Fe_{0.2}$–N–C-224; (b) $Zn_{0.5}Fe_{0.5}$–N–C-224; (c) $Zn_{0.5}Fe_{0.5}$–N–C-222.
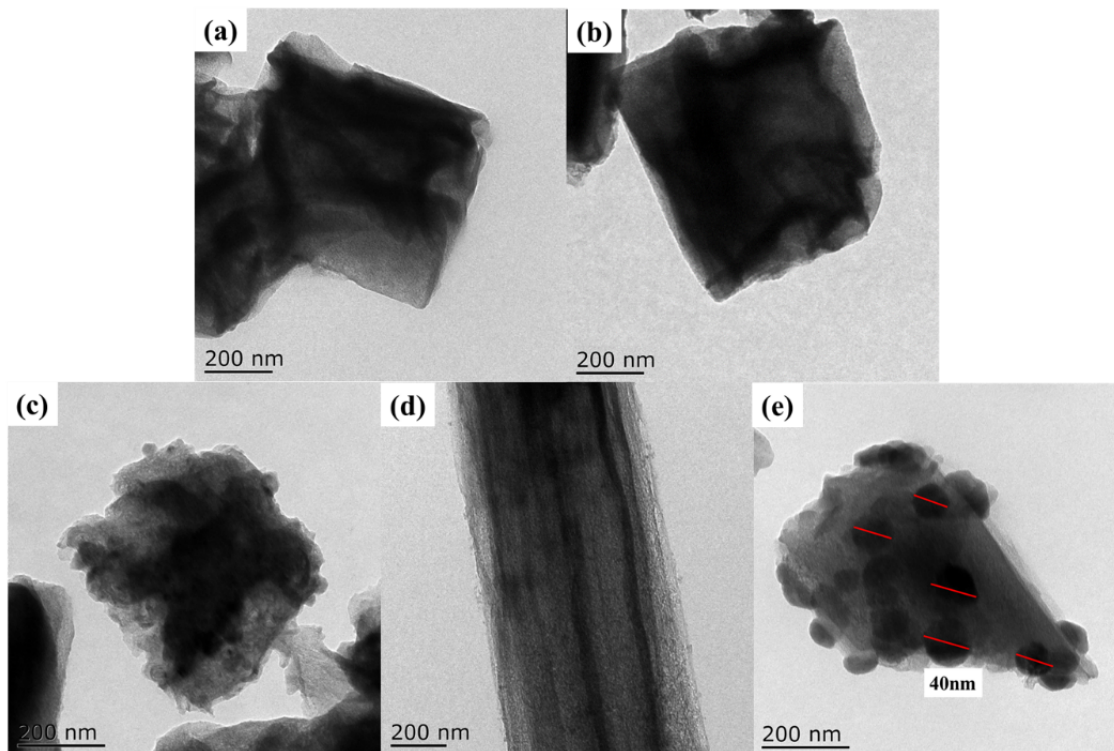
Figure S6. TEM images of each Zn_xFe_y–N–C catalyst: (a) Zn_1Fe_0–N–C-224; (b) $Zn_{0.8}Fe_{0.2}$–N–C-224; (c) $Zn_{0.5}Fe_{0.5}$–N–C-224; (d) $Zn_{0.5}Fe_{0.5}$–N–C-222; (e) Zn_0Fe_1–N–C-224.
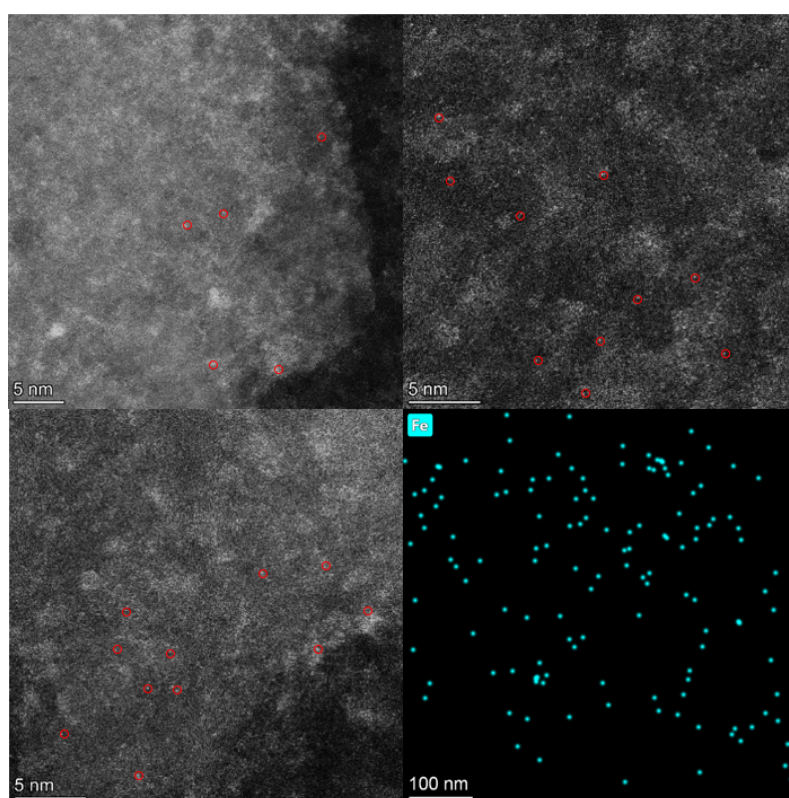
Figure S7. Aberration-corrected STEM images of $Zn_{0.5}Fe_{0.5}$–N–C-224.
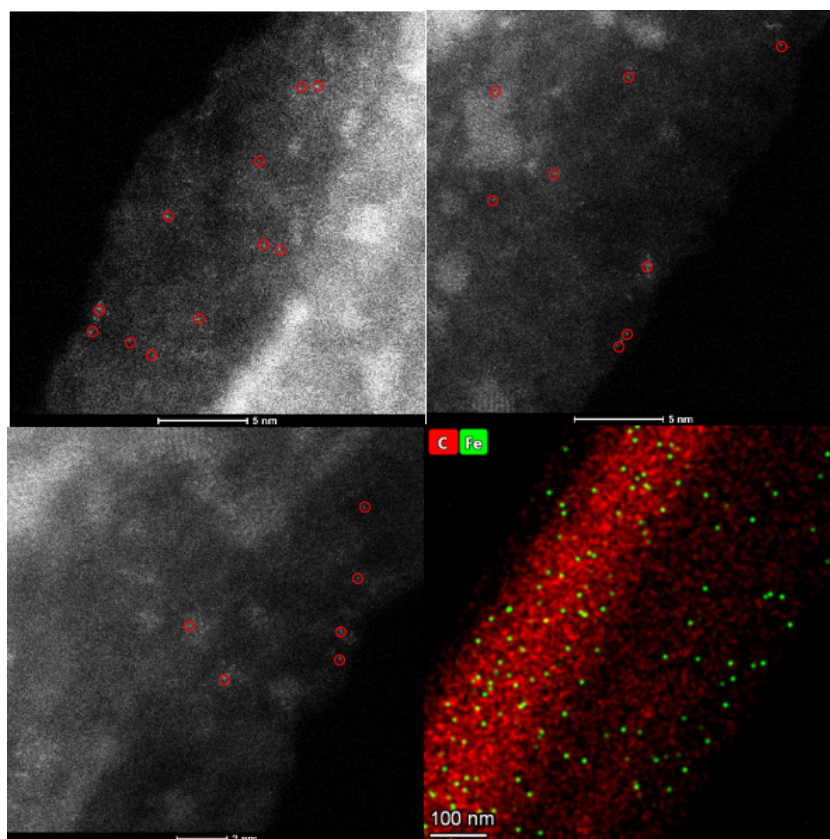
Figure S8. Aberration-corrected STEM images of $Zn_{0.5}Fe_{0.5}$–N–C-222.
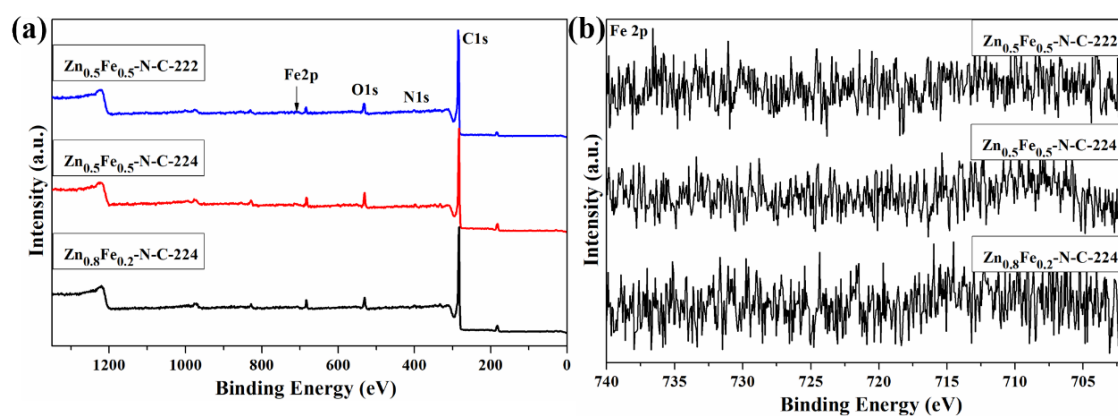
Figure S9. XPS spectra of $Zn_{0.5}Fe_{0.5}$–N–C-224, $Zn_{0.8}Fe_{0.2}$–N–C-224 and $Zn_{0.5}Fe_{0.5}$–N–C-222: (a) Survey spectra; (b) Fe 2p.
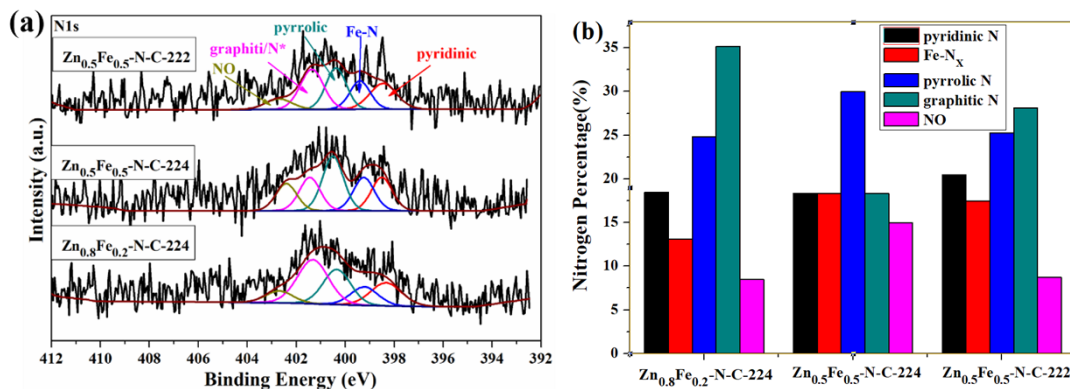
Figure S10. XPS spectra of $Zn_{0.5}Fe_{0.5}$–N–C-224, $Zn_{0.8}Fe_{0.2}$–N–C-224, and $Zn_{0.5}Fe_{0.5}$–N–C-222 catalysts: (a) N 1s; (b) Percentage of different N species in N_{total} (%).

Table S4. Percentage of different N species on the surface of the three Zn_xFe_y–N–C materials analyzed by XPS in N_{total}

Sample	N_{total}	Pyridinic-N/N_{total}	$Fe-N_x$/N_{total}	Pyrrolic/N_{total}	graphitic/N*/N_{total}	NO/N_{total}
$Zn_{0.8}Fe_{0.2}$–N–C-224	2.54	18.46	13.08	24.83	35.15	8.47
$Zn_{0.5}Fe_{0.5}$–N–C-224	2.42	18.34	18.35	29.97	18.36	14.98
$Zn_{0.5}Fe_{0.5}$–N–C-222	3.38	20.44	17.43	25.27	28.13	8.72
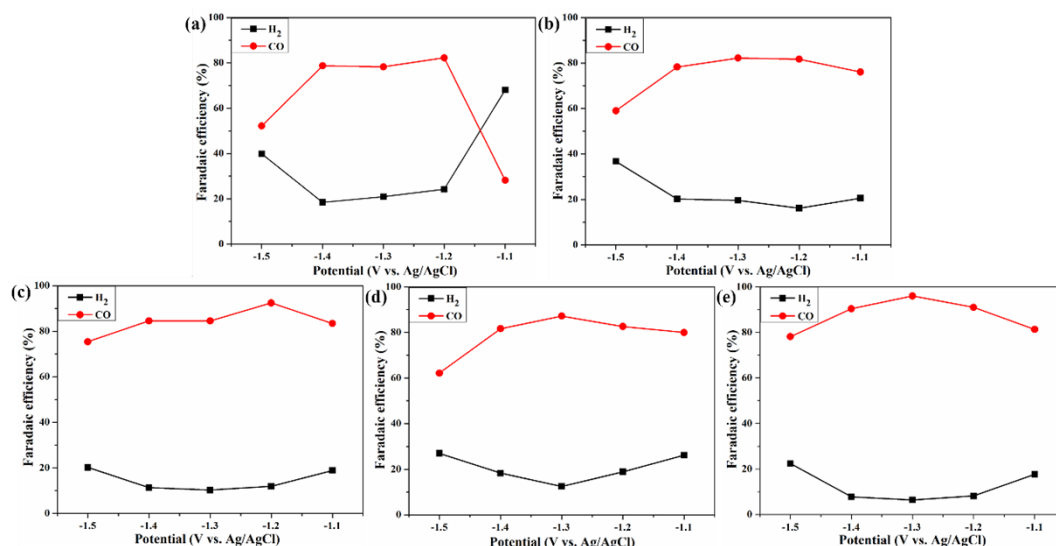
Figure S11. Faraday efficiency of main gas phase products of each Zn_xFe_y–N–C catalyst at $-1.1 \sim -1.5$ V vs. Ag/AgCl potential (the loading capacity is 2.5 mg cm^{-2}): (a) Zn_1Fe_0–N–C-224; (b) $Zn_{0.8}Fe_{0.2}$–N–C-224; (c) $Zn_{0.5}Fe_{0.5}$–N–C-224; (d) Zn_0Fe_1–N–C-224; (e) $Zn_{0.5}Fe_{0.5}$–N–C-222.

Table S5. List of the CO_2ER performance of Fe SAs based Fe–N–C materials in the literature

Catalyst	Fe	Fe-N	Electrolyte/	Potential	FE_{CO}	Stability test	Recyclabili	Ref

	content wt.% (ICP)	coordination	KHCO$_3$	vs. RHE /V		time and FE$_{CO}$ performance	ty, FE$_{CO}$	
Zn$_{0.5}$Fe$_{0.5}$-N-C-222	1.04	Fe-N$_4$		−0.70	96%	12 h, ~90%	6 times, >86%	This work
Zn$_{0.5}$Fe$_{0.5}$-N-C-224	1.06	Fe-N$_4$	0.1 M	−0.60	93%	12 h, >91%	8 times, >93%	
C-AFC©ZIF-8	1.47	----	1.0 M	−0.43	93%	----	----	S1
Fe/NG-750	0.52	Fe-N$_4$	0.1 M	−0.60	80%	10 h, ~80%	----	S2
Fe-N-C	0.1[N1]	Fe-N$_4$	0.1 M	−0.58	93%	20.2 h, >93%	----	S3
Fe-N-PC[N2]	3.9	----	0.5 M	−0.49	90%	----	----	S4
rGO-PVP-ZIFc	0.16	----	0.5 M	−0.62	98%	8 h, ~98%	----	S5
FeN$_5$	1.44[N1]	Fe-N$_5$	0.1 M	−0.46	97%	24 h, ~97%	----	S6
Fe-N-C-0.5	----	Fe-N$_4$	0.5 M	−0.64	95%	----	----	S7
axial Fe-N/CNT	2.68	----	0.5 M	−0.60	95%	10 h, ~95%	----	S8
FeSAs/CNF-900	4.58	Fe-N$_4$	0.5 M	−0.47	87%	12 h, >80%	----	S9
Fe-N/O-C(MZ)	0.15	Fe-N$_4$	0.1 M	−0.57	96%	22 h, 95~96%	----	S10
SA-Fe/NG-600	----	----	0.5 M	−0.50	97%	10 h, >90%	----	S11
DNG-SAFe	0.71	Fe-N$_4$	0.1 M	−0.85	90%	20 h, 87~94%	----	S12
Fe-SA/NCS-700	0.89[N1]	----	0.5 M	−0.45	87%	10 h, ~87%	-----	S13
FeN$_4$/C	1.2	Fe-N$_4$	0.1 M	−0.60	93%	24 h, >80%	-----	S14
Fe-N/CNT@GNR	1.75	Fe-N$_4$	0.1 M	−0.76	98%	5 h, >95%		S15

N1: Surficial atomic concentration of Fe observed from XPS

N2: Coexistence of Fe clusters.

Table S6. R_{cell} and R_{ct} of each catalyst obtained by impedance test

Catalyst	R_{cell}	R_{ct}
Zn$_1$Fe$_0$-N-C-224	11.90	8.04
Zn$_{0.8}$Fe$_{0.2}$-N-C-224	11.17	4.32
Zn$_{0.5}$Fe$_{0.5}$-N-C-224	11.61	5.01
Zn$_0$Fe$_1$-N-C-224	10.45	4.96
Zn$_{0.5}$Fe$_{0.5}$-N-C-222	12.24	4.90
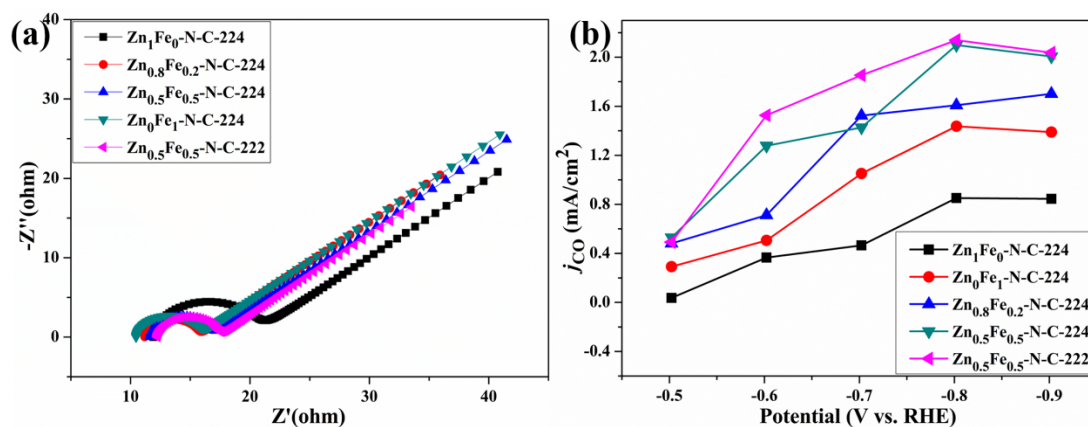
Figure S12. (a) Impedance spectra of each catalyst at −1.3 V vs. Ag/AgCl; (b) Partial current density of CO at different potentials.
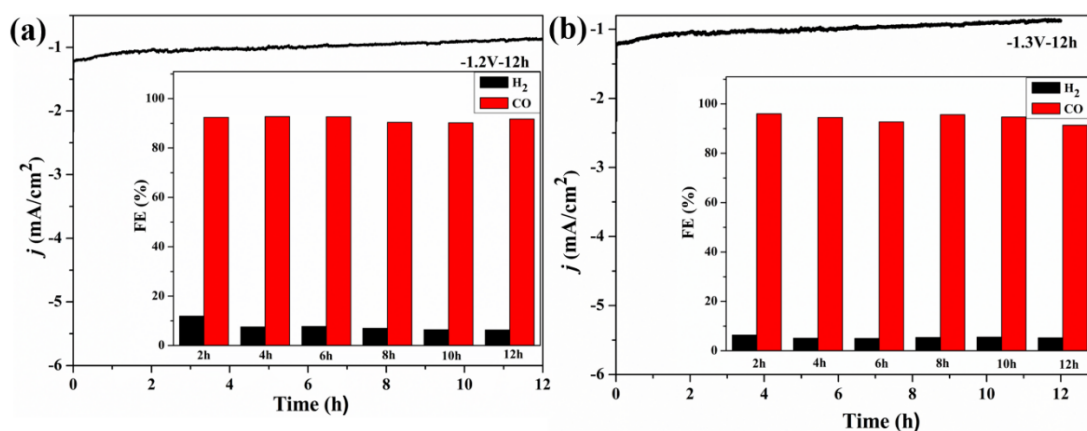
Figure S13. The i-t curve of the catalyst modified electrode (loading 2.5 mg cm^{-2}) for 12 h electrolysis and the relationship between product efficiency and time (insert): (a) Zn$_{0.5}$Fe$_{0.5}$–N–C-224 at −1.2 V vs. Ag/AgCl; (b) Zn$_{0.5}$Fe$_{0.5}$–N–C-222 at −1.3 V vs. Ag/AgCl.

To further investigate the origin catalytic mechanism of the Fe–N$_x$ on CO$_2$RR, we conducted the DFT calculation. Four kinds of coordination environments of Fe–N$_x$ (x=1~4) were employed as models for drawing the free energy profiles of transfer CO$_2$ to CO based on the steps of (1) CO$_2$ + * + H$^+$+ e$^-$→*COOH; (2) *COOH+ H$^+$+ e$^-$ →*CO + H$_2$O; and (3) *CO→CO+* (Fig. S14–S17). The *CO desorption step is the rate-determining step in all models with an approximately increasing ΔG from x=4 to x=1, that is, 0.71, 1.18, 1.70, and 1.73 eV for Fe–N$_4$, Fe–N$_3$, Fe–N$_2$, and Fe–N$_1$, respectively (Fig. S18).
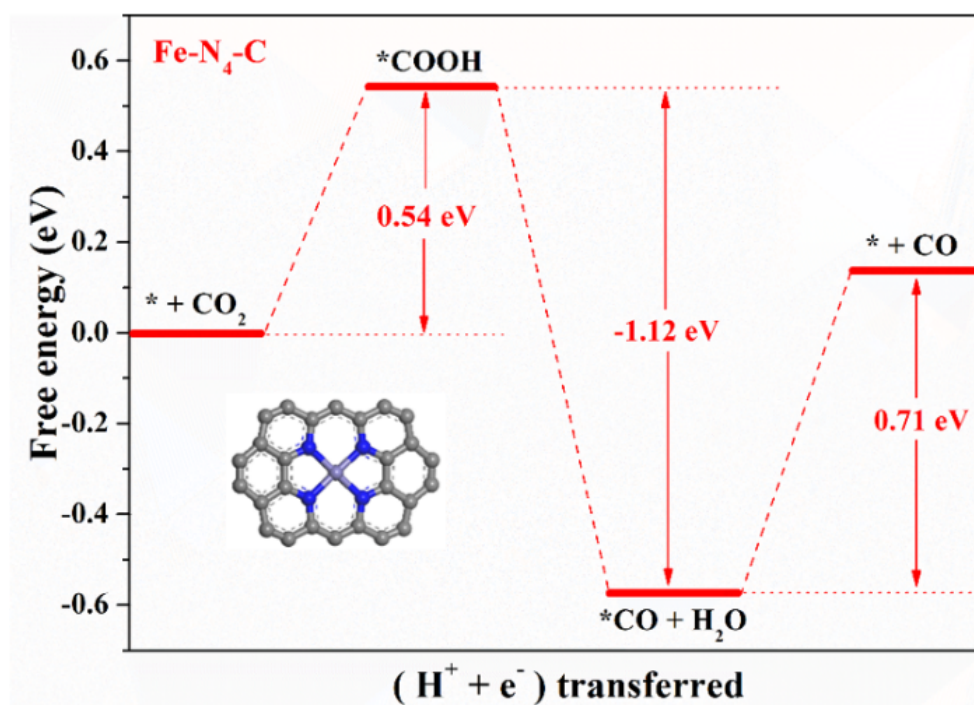
Figure S14. Free energy profiles for electrochemical reduction of CO_2 to CO on Fe-N_4-C model.
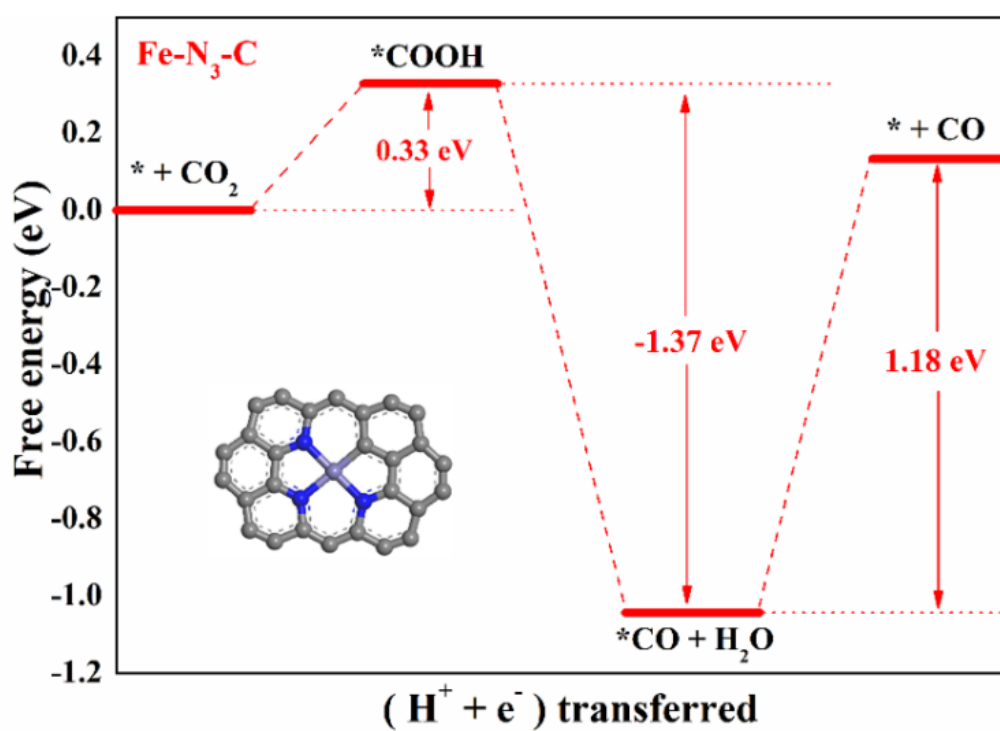
Figure S15. Free energy profiles for electrochemical reduction of CO_2 to CO on Fe-N_3-C model.
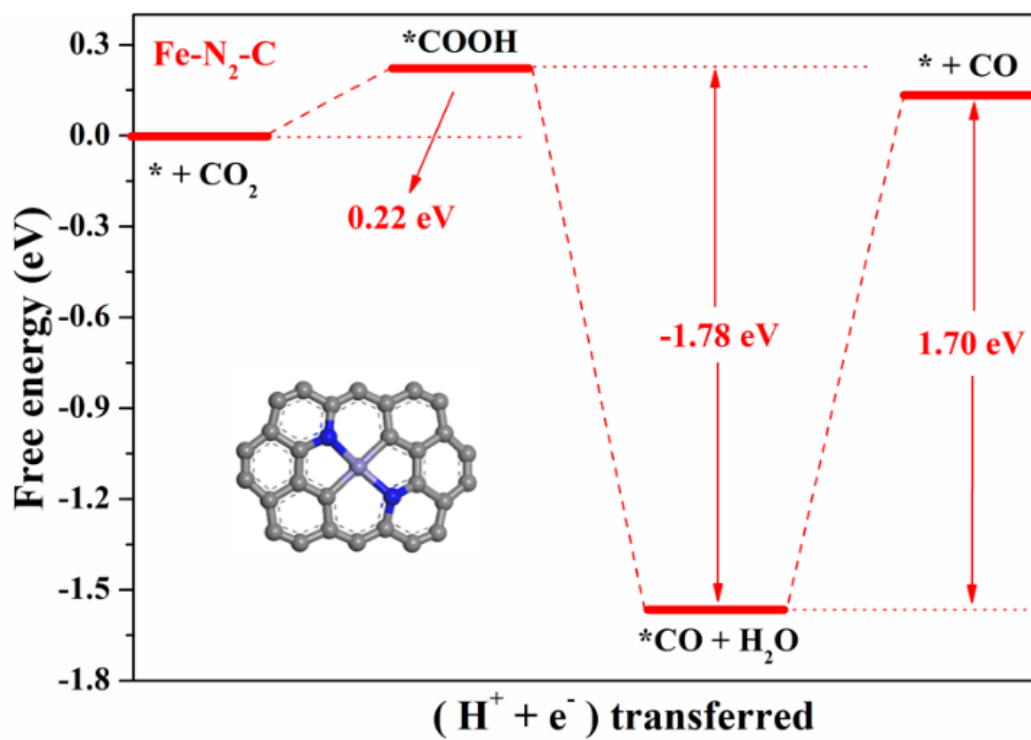
Figure S16. Free energy profile for electrochemical reduction of CO_2 to CO on Fe-N_2-C model.
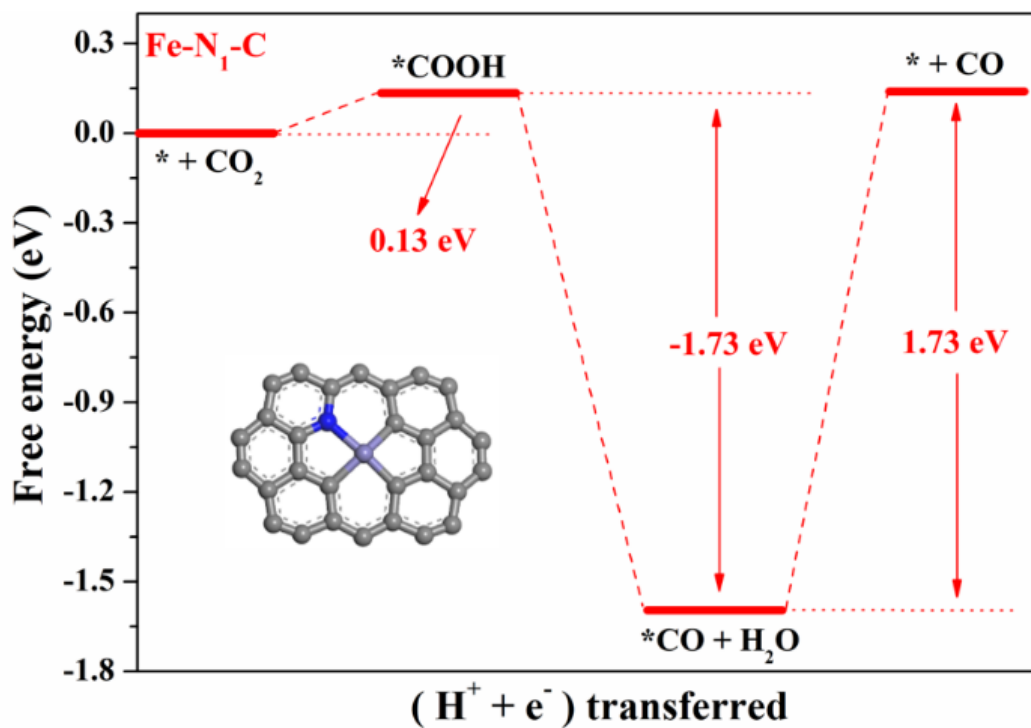
Figure S17. Free energy profile for electrochemical reduction of CO_2 to CO on Fe-N-C model.
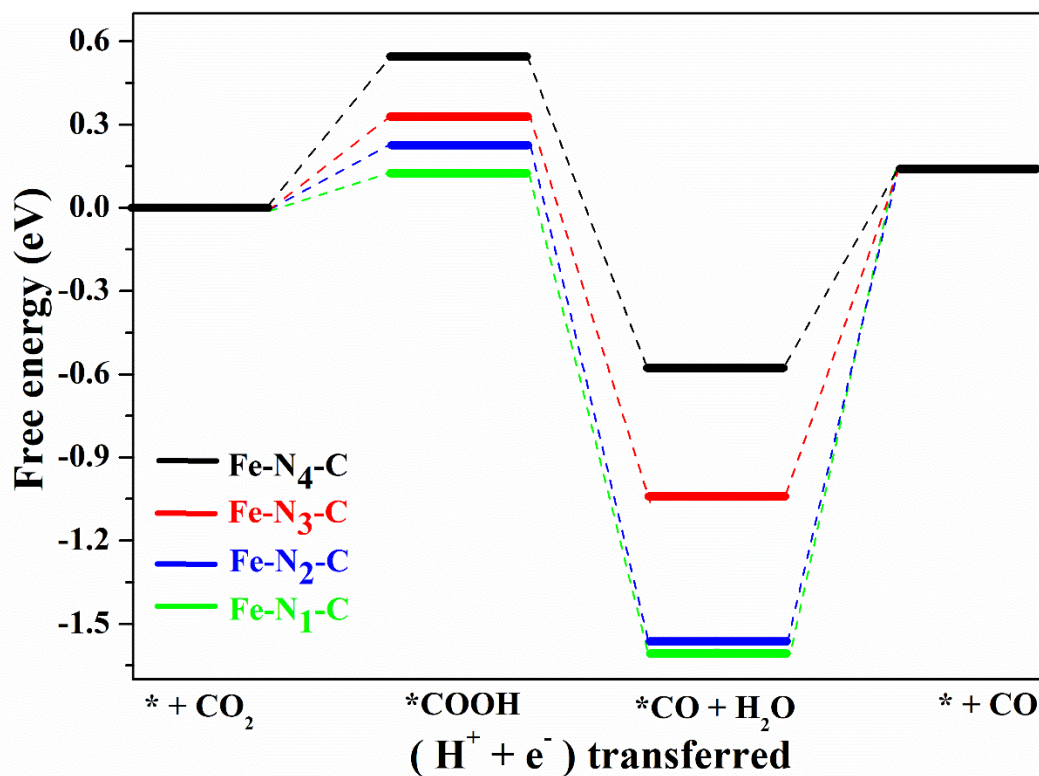
Figure S18. Free energy profiles for the CO_2ER on each Fe-N_x-C model.
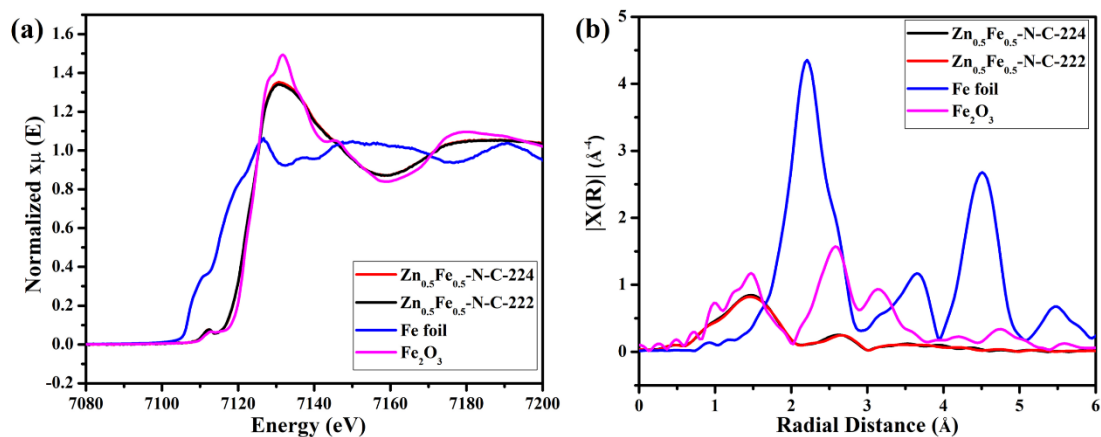
Figure S19. (a) The comparison of Fe K-edge XANES spectra. (b) The comparison of Fe K-edge EXAFS, shown in k^3 weighted R-space.
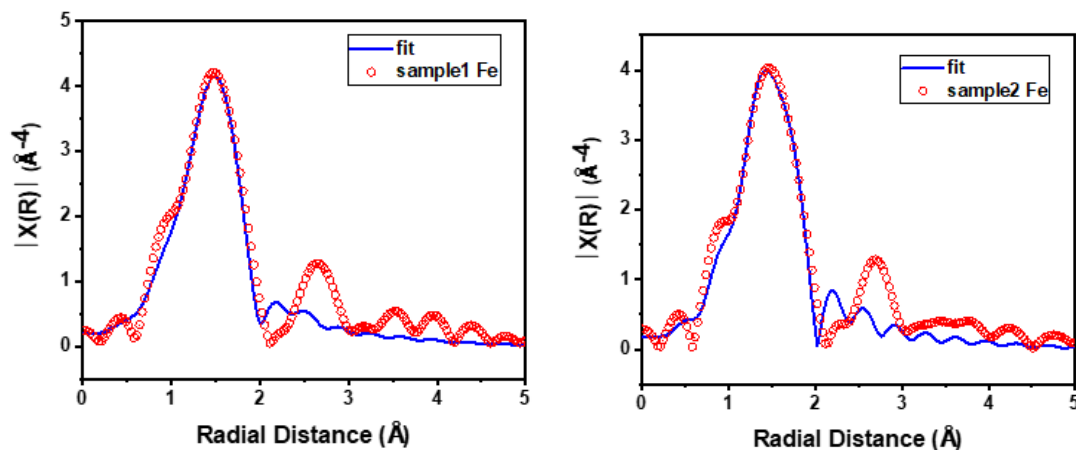
Figure S20. Fe K-edge EXAFS (points) and fit (line) for $Zn_{0.5}Fe_{0.5}$–N–C-224 (left) and $Zn_{0.5}Fe_{0.5}$–N–C-222 (right), shown in k^3 weighted R-space.

Experimental

Synthesis of the precursors

Synthesis of PCN-224(Zn_xFe_y) (x and y are the molar ratios of Zn–TCPP and Fe–TCPP ligands, which are 1, 0; 0.8, 0.2; 0.5, 0.5; 0, 1, respectively). Take the synthesis of PCN-224(Zn_1Fe_0) as an example, $ZrCl_4$ (120 mg), Zn–TCPP (40 mg), Fe–TCPP (0 mg), and CH_3COOH (0.5 mL) in 7.5 mL of DMF (*N, N*-dimethylformamide) were ultrasonically dissolved in a 20 mL Pyrex vial. The mixture was heated at 120 °C for 12 h. After cooling down to room temperature, the obtained purple products were separated by centrifugation. Subsequently, they were washed (with DMF 3 times and

acetone twice) and dried at 80 °C in a vacuum overnight. The synthesis processes of PCN-224($Zn_{0.8}Fe_{0.2}$), PCN-224($Zn_{0.5}Fe_{0.5}$), and PCN-224(Zn_0Fe_1) are similar to that of PCN-224(Zn_1Fe_0), except that the mass ratio of ligands is different.

The synthesis of PCN-222($Zn_{0.5}Fe_{0.5}$) was employed with the following dosage: $ZrCl_4$ (120 mg), Zn–TCPP (20 mg), Fe–TCPP (20 mg), and CH_3COOH (0.5 mL) were dissolved in 8.0 mL of DMF. The subsequent treatment is the same as the above-mentioned.

Synthesis of Zn_xFe_y–N–C catalysts

Typically, precursors were heated from room temperature to 1000 °C with a heating rate of 5 °C min^{-1}, then pyrolyzed at this temperature for 1 h in N_2 atmosphere. Subsequently, the ZrO_2 involved in the resultant product was removed by immersing the sample in HF (50wt%) solution for 6 h at 60 °C. The black sample was collected by centrifugation, washed several times with distilled water and ethanol, and dried at 80 °C under vacuum overnight. According to different ratios of free ligands in the precursors, pyrolysis products of Zn_xFe_y–N–C were obtained, which are expressed as Zn_1Fe_0–N–C-224, $Zn_{0.8}Fe_{0.2}$–N–C-224, $Zn_{0.5}Fe_{0.5}$–N–C-224, Zn_0Fe_1–N–C-224, and $Zn_{0.5}Fe_{0.5}$–N–C-222, respectively.

Material characterization

A Bruker D8 Advance X-ray diffractometer detector with Cu Kα radiation was used for the X-ray diffraction (XRD) characterization. Thermal gravimetric analyses were performed on a TG/DSC Model STA 449 F3 Netzsch instrument under argon (10 ºC min^{-1}). Scanning electron microscopy (SEM) and the energy-dispersive X-ray spectroscopy (EDS) measurements were recorded on a Hitachi 4800 microscopy. Transmission electron microscopy (TEM) was performed on Holland Philips Tecnai 12 microscopy. High power transmission electron microscopy (HRTEM) images were obtained using Tecnai G2 F30 field emission transmission electron microscopy from FEI Corporation, USA. Use objective spherical aberration-corrected transmission electron microscope (FEI-Themis Z) to measure Fe single atoms. X-ray photoelectron spectroscopy (XPS) was measured using a Thermo Scientific ESCALAB 250Xi. N_2 adsorption-desorption isotherms and pore size distribution were obtained on a

Micromeritics ASAP 2020 HD88 Surface Area and Porosity Analyzer. Elemental analyses for C, H, and N were collected on a PerkinElmer 240C analyzer. The content of Fe was measured using an Inductively Coupled Plasma Emission Spectrometer (ICP-OES DV7300, USA, PerkinElmer).

X-ray absorption spectrum

The Fe K-edge X-ray absorption near edge structure (XANES) and extended X-ray absorption fine structure (EXAFS) experiments were carried out at the beamlines 5BM-D and 20BM-B of Advanced Photon Source (APS) at Argonne National Laboratory (ANL). All data were collected in the fluorescence mode due to low Fe concentration. EXAFS fitting is applied through Athena and Artemis software (Table S7).[S16]

Table S7. Fitting parameters for Fe K-edge EXAFS

Sample	Paths	CN	R	σ
$Zn_{0.5}Fe_{0.5}$–N–C-224	Fe-N	3.9±0.3	1.95	0.007
	Fe-O	2.1±0.2	2.07	0.004
$Zn_{0.5}Fe_{0.5}$–N–C-222	Fe-N	4.1±0.2	1.95	0.005
	Fe-O	1.9±0.1	2.08	0.001

Electrochemistry measurements and product analyses

Electrochemical CO_2 reduction measurements were carried out on CHI 660 electrochemical workstation at 25 °C. For a conventional three-electrode system, a Pt sheet was used as the counter electrode. The reference electrode is Ag/AgCl, which is stored in a saturated KCl aqueous solution before use. The as-synthesized Zn_xFe_y–N–C was utilized as the working electrode. To prepare the catalyst ink, a 30 mg sample was scattered in a mixture of 400 μL H_2O, 200 μL Nafion solution (5wt%), and 400 μL isopropanol, followed by ultrasonic and stirring for 12 h to obtain the uniform catalyst suspension. The ink was brush coated on the carbon paper (1.0 cm × 1.0 cm) and then dried in the air (2.5 mg cm^{-2} loading was obtained).

A custom H-type glass cell was employed in this work, which has 160 mL volume for both sides and a cation exchange membrane of Nafion®112 for separation. Both

compartments were filled with a 60.0 mL 0.1 M $KHCO_3$ solution as the electrolyte. Before electrolysis, high purity (99.999%) of CO_2 was fed into the cathode chamber for 30 min until the electrolyte was saturated (pH=6.77). Linear voltammetry tests (LSV) were performed in the range of –1.5 to 0.5 V vs. Ag/AgCl. The chronopotentiometry was measured in the potential range from –1.1 to –1.5 V vs. Ag/AgCl for 2 h.

After electrolysis, the gaseous products of H_2 and CO were detected by the thermal conductivity detector (TCD) in Gas Chromatography (SP-7890) using the TDX–01 column. H_2 and CO standard curves are presented in Fig. S21.
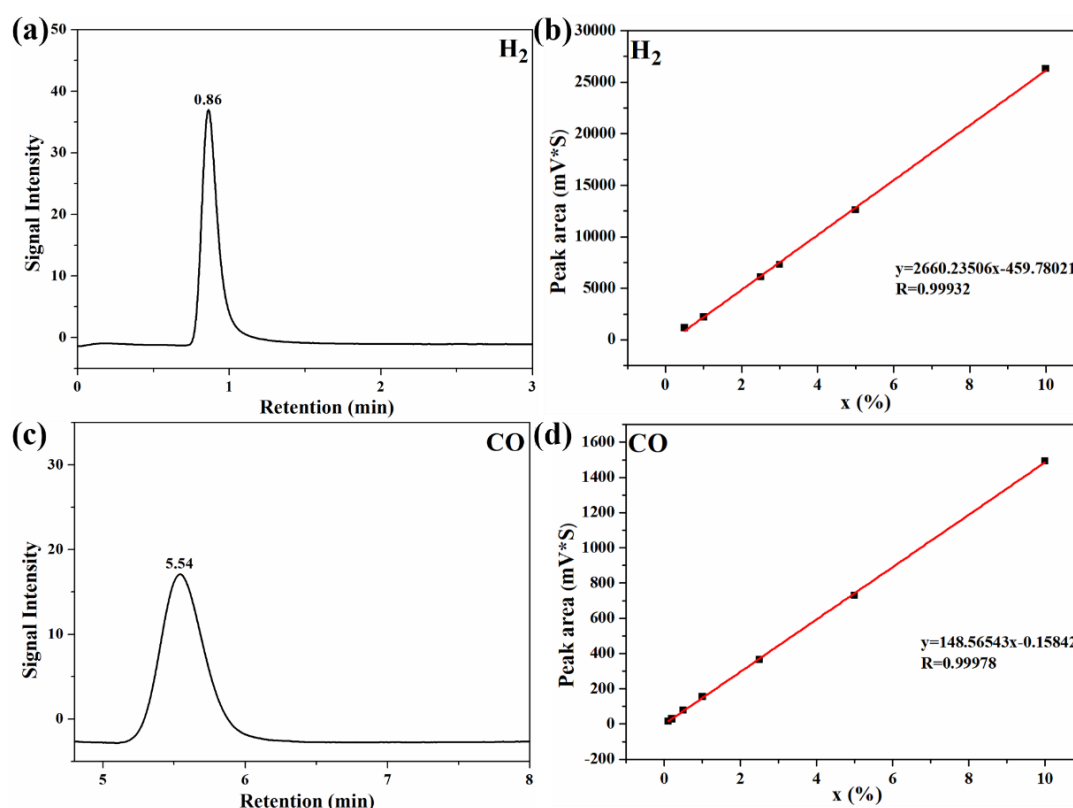
Figure S21. Chromatographic peaks (a, c) and standard curves (b, d) for pure hydrogen and CO established on the TDX-01 column for GC analysis.

DFT calculations

All calculations adopt the spin-polarized density functional method within DMol[3] code of Materials Studio.[S17, S18] We selected the Perdew-Burke-Ernzerhof (PBE) of the generalized gradient approximation (GGA) to describe the electron interactions.[S19] For the transition metals, we employed the DFT Semi-core Pseudopotential (DSPP)

method, while for other elements we used the double numerical plus d-functions (DND) basis set.[S20] The energy, force, and displacement convergence criteria were set as 2×10^{-5} Ha, 4×10^{-3} Ha/Å, and 5×10^{-3} Å in all DFT calculations, respectively. The Gibbs free energy change (ΔG) of every step was obtained by applying the computational hydrogen electrode (CHE) model proposed by Nørskov et al.[S21, S22] The ΔG and free energy were calculated as:

$$\Delta G_{*COOH} = G_{*COOH} - G_{*} - G_{CO2} - 1/2 G_{H2} \tag{1}$$

$$G = E + E_{ZPE} - TS \tag{2}$$

where E is the electronic energy calculated by DFT, T is the temperature; E_{ZPE} and S are the zero-point energy and entropy, respectively, estimated under harmonic approximation from the frequency analysis.

Stability test of $Zn_{0.5}Fe_{0.5}$–N–C-222 catalyst at a low loading

When applying a low load capacity of 1.5 mg cm^{-2} of $Zn_{0.5}Fe_{0.5}$–N–C-222 for the electrolysis test, we obtained a uniform catalyst covering in the carbon paper thanks to its lower power density. It could reach a maximum FE_{CO} of 96% at -1.3 V vs. Ag/AgCl and maintain the average current density of 1.91 mA cm^{-2} (Fig. S22). This merit is desirable for the industrial application, especially for the catalyst which possesses high selectivity, super-stability, and low cost at the same time.
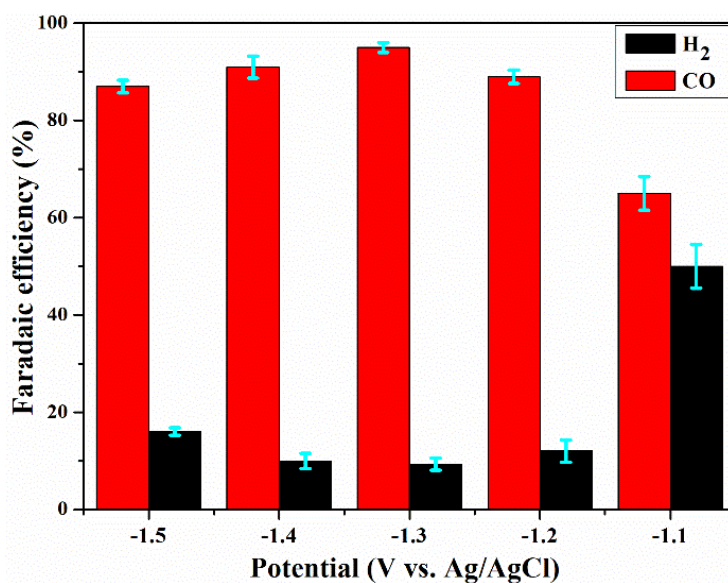
Figure S22. Faraday efficiency of $Zn_{0.5}Fe_{0.5}$–N–C-222 catalyst with a loading of 1.5 mg cm^{-2}.

We tentatively ascribe their superior performance to the consequence of adopting the mixed-ligand strategy. Different from the catalyst prepared by Jiang *et al.* which demonstrated a high content of Fe SAs of 1.76 wt%, such attempts are conducive to the maximum utilization of active sites even with a medium content of 1.04–1.06 wt% since the Fe content is not always proportional to the FE_{CO} in different Fe SACs (Table S5). We also carried out the control experiment by using the catalysts of Zn-free, Zn_0Fe_1–N–C-224, and Zn_0Fe_1–N–C-222, respectively, which display 87% and 82% of maximum FE_{CO}, as well as decreasing production of CO (reach to 72%) and increasing H_2 production (reach to 18~19%) during 12 h electrolysis process (Fig. S23–S24). It hints that excess introduction of Fe would induce the generation of Fe NPs and result in a fierce competition of HER.

Figure S23. Th[...]/AgCl and the relationshi[...]

Figure S24. The i-t curve of Zn_0Fe_1–N–C-222 for 12 h electrolysis at –1.3 V vs. Ag/AgCl and the relationship between product efficiency and time (insert).

References

[S1] Y. Ye, F. Cai, H. Li, H. Wu, G. Wang, Y. Li, S. Miao, S. Xie, R. Si, J. Wang, X. Bao. Surface functionalization of ZIF-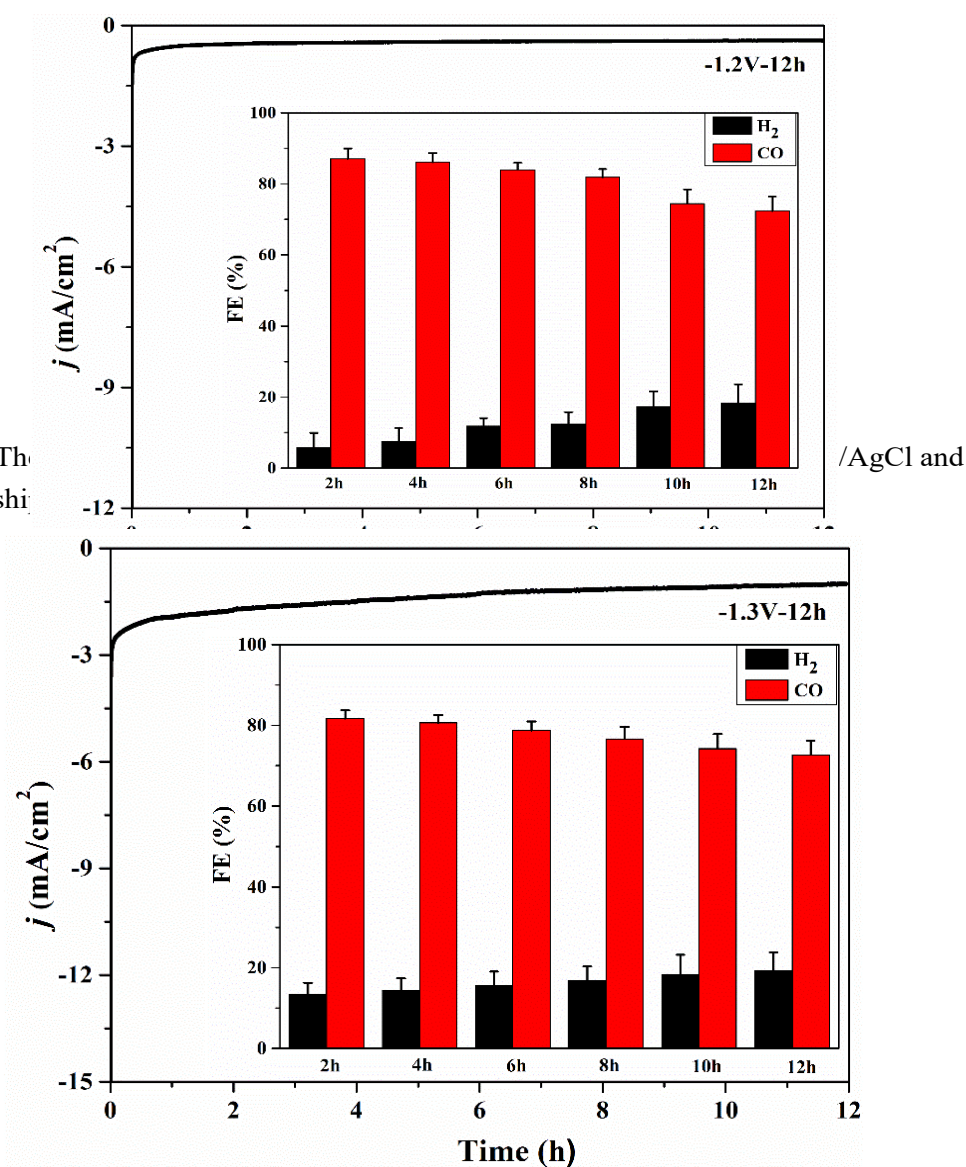8 with ammonium ferric citrate toward high exposure of Fe-N active sites for efficient oxygen and carbon dioxide electroreduction. *Nano Energy*, 2017, **38**, 281–289.

[S2] C Zhang, S. Yang, J. Wu, M. Liu, S. Yazdi, M. Ren, J. Sha, J. Zhong, K. Nie, A. S. Jalilov, Z. Li, H. Li, B. I. Yakobson, Q. Wu, E. Ringe, H. Xu, P. M. Ajayan, J. M. Tour, Electrochemical CO_2 reduction with atomic iron-dispersed on nitrogen-doped graphene. *Adv Energy Mater,* 2018, **8**,1703487.

[S3] F. Pan, H. Zhang, K. Liu, D. Cullen, K. More, M. Wang, Z. Feng, G. Wang, G. Wu, Unveiling active sites of CO_2 reduction on nitrogen-coordinated and atomically dispersed iron and cobalt catalysts. *ACS Catal*. 2018, **8**, 3116−3122.

[S4] Y. Chen, L. Zou, H. Liu, C. Chen, Q. Wang, M. Gu, B. Yang, Z. Zou, J. Fang, H. Yang, Fe and N Co-doped porous carbon nanospheres with high density of active sites for efficient CO_2 electroreduction. *J Phys Chem C*, 2019, **123**, 16651−16659.

[S5] C. Hu, Y. Mu, S. Bai, J. Yang, L. Gao, S. D. Cheng, S. B. Mi, J. Qiu, Polyvinyl pyrrolidone mediated fabrication of Fe, N-codoped porous carbon sheets for efficient electrocatalytic CO_2 reduction. *Carbon*, 2019, **153**, 609−616.

[S6] H. Zhang, J. Li, S. Xi, Y. Du, X. Hai, J. Wang, H. Xu, G. Wu, J. Zhang, J. Lu, J. Wang, Graphene supported single-atom FeN_5 catalytic site for efficient electrochemical CO2 reduction, *Angew. Chem. Int. Ed*., 2019, 58, 14871–14876.

[S7] S. Wu, X. Lv, D. Ping, G. Zhang, S. Wang, H. Wang, X. Yang, D. Guo, S. Fang, Highly exposed atomic Fe-N active sites within carbon nanorods towards electrocatalytic reduction of CO_2 to CO. *Electrochim Acta*, 2020, **340**, 135930.

[S8] J. Tuo, Y. Lin, Y. Zhu, H. Jiang, Y. Li, L. Cheng, R. Pang, J. Shen, L. Song, C. Li, Local

structure tuning in Fe-N-C catalysts through support effect for boosting CO_2 electroreduction. *Appl Catal B*, 2020, **272**, 118960.

[S9] X. Chen, D. D. Ma, B. Chen, K. Zhang, R. Zou, X. T. Wu, Q. L. Zhu, Metal–organic framework-derived mesoporous carbon nanoframes embedded with atomically dispersed Fe–N_x active sites for efficient bifunctional oxygen and carbon dioxide electroreduction. *Appl Catal B*, 2020, **267**, 118720.

[S10] X. Wang, Y. Pan, H. Ning, H. Wang, D. Guo, W. Wang, Z. Yang, Q. Zhao, B. Zhang, L. Zheng, J. Zhang, M. Wu, Hierarchically micro- and meso-porous $Fe-N_4O$-doped carbon as robust electrocatalyst for CO_2 reduction. *Appl Catal B*, 2020, **266**, 118630.

[S11] J. Tuo, Y. Zhu, H. Jiang, J. Shen, C. Li, The effect of the coordination environment of atomically dispersed Fe and N Co-doped carbon Nanosheets on CO_2 electroreduction. *ChemElectroChem*, 2020, **7**, 4767-4772.

[S12] W. Ni, Z. Liu, Y. Zhang, C. Ma, H. Deng, S. Zhang, S. Wang, Electroreduction of carbon dioxide driven by the intrinsic defects in the carbon plane of a single $Fe–N_4$ site. *Adv Mater*, **2020**, 2003238.

[S13] Y. Zhu, X. Li, X. Wang, K. Lv, G. Xiao, J. Feng, X. Jiang, M. Fang, Y. Zhu, Single-atom iron-nitrogen catalytic site with graphitic nitrogen for efficient electroreduction of CO_2. *ChemistrySelect*, **2020**, 5, 1282-1287.

[S14] X. Li, S. Xi, L. Sun, S. Dou, Z. Huang, T. Su, X. Wang, Isolated FeN_4 sites for efficient electrocatalytic CO_2 reduction. *Adv. Sci.* **2020**, 7, 2001545.

[S15] F. Pan, B. Li, E. Sarnello, Y. Fei, Y. Gang, X. Xiang, Z. Du, P. Zhang, G. Wang, H. T. Nguyen, T. Li, Y. Hu, H. Zhou, Y. Li, Atomically dispersed iron-nitrogen sites on hierarchically mesoporous carbon nanotube and graphene nanoribbon networks for CO_2 reduction. *ACS Nano*, **2020**, 14, 5506-5516.

[S16] B. Ravel, M. Newville, ATHENA, ARTEMIS, HEPHAESTUS: data analysis for X-ray absorption spectroscopy using IFEFFIT. *J. Synchrotron Radiat*, **2005**, 12(4), 537-541.

[S17] B. Delley, An all-electron numerical method for solving the local density functional for polyatomic molecules, *J. Chem. Phys*. **1990**, 92, 508–517.

[S18] B. Delley, From molecules to solids with the $DMol^3$ approach, *J. Chem. Phys*. **2000**, 113, 7756–7764.

[S19] J. P. Perdew, K. Burke, M. Ernzerhof, Generalized gradient approximation made simple, *Phys. Rev. Lett.* **1996**, 77, 3865–3868.

[S20] B. Delley, Hardness conserving semilocal pseudopotentials, *Phys. Rev. B*. **2002**, 66(15), 155125–155133.

[S21] J. K. Nørskov, J. Rossmeisl, A. Logadottir, L. Lindqvist, J. R. Kitchin, T. Bligaard, H. Jónsson, Origin of the overpotential for oxygen reduction at a fuel–cell cathode, *J. Phys. Chem. B*. **2004**, 46, 17886–17892.

[S22] J. Rossmeisl, A. Logadottir, J. K. Nørskov, Electrolysis of water on (oxidized) metal surfaces, *Chem. Phys*. **2005**, 319(1–3), 178–184.